ACTA IMEKO
ISSN: 2221-870X
December 2024, Volume 13, Number 4, 1 - 8

A simple experimental method to estimate and benchmark automotive LIDARs performance in fog

Davide Cassanelli[1], Stefano Cattini[1], Lorenzo Medici[2], Luca Ferrari[2], Luigi Rovati[1]

[1] *Department of Engineering, "Enzo Ferrari" University of Modena and Reggio Emilia, 41125 Modena, Italy*
[2] *CNH Industrial Italia S.p.A, Italy*

ABSTRACT
LiDARs hold promise for various automotive applications, but their performance in adverse weather conditions remains a severe limitation. Indeed, fog can compromise the ability to perform fundamental tasks such as detection, classification, and tracking. The success of these tasks depends on the quality of the data provided by the LiDAR, i.e., the point cloud, PC, and the algorithms used to analyse that PC. Some previous studies exploited large and sophisticated facilities filled with fog to analyse LiDARs in fog. However, such facilities are intrinsically highly complex and costly. To overcome these limitations, we propose a much less expensive method based on a fog chamber, a 1 m side transparent chamber to be placed between the LiDAR and the targets, then filled with fog. The proposed method allows for the analysis and comparison of the performance of both LiDARs and processing algorithms while avoiding the cost and complexity of large facilities and the limitations intrinsic to mathematical modelling and numerical simulation. To provide examples of the information that is obtainable using the proposed method, the results from a popular LiDAR and processing algorithm, namely, the Velodyne VLP 16, and the MATLAB® Computer Vision Toolbox, are also reported.

Section: RESEARCH PAPER

Keywords: LiDAR; fog; bad weather conditions; automotive sensors; autonomous driving; optical sensors; ADAS

Citation: D. Cassanelli, S. Cattini, L. Medici, L. Ferrari, L. Rovati , A simple experimental method to estimate and benchmark automotive LIDARs performance in fog, Acta IMEKO, vol. 13 (2024) no. 4, pp. 1-8. DOI: 10.21014/actaimeko.v13i4.1885

Section Editor: Laura Fabbiano, Politecnico di Bari, Italy

Received May 29, 2024; **In final form** November 11, 2024; **Published** December 2024

Corresponding author: Davide Cassanelli, e-mail: davide.cassanelli@unimore.it

1. INTRODUCTION

The present and future of the automotive industry are strictly related to autonomous driving. As a result, the research and economic interest in measuring systems aimed at supporting ADAS has significantly grown in recent years, promoting the proliferation of manufacturers and commercial systems. Among the measuring systems that have seen a significant increase in terms of technologies, manufacturers, and models, LiDARs certainly hold a relevant place. In light of this, several recent studies have been proposed to allow the performance of LiDARs to be analysed and compared e.g. [1]-[6]. Such studies mainly treat the analysis and characterisation of LiDARs in optimal weather conditions, that is, good visibility. However, adverse weather conditions (fog, rain, snow) may severely affect the LiDAR performances. Accordingly, in this study, we focus on the development of an experimental method that allows evaluating the impact of fog both on the LiDAR performance, i.e., quality of the point clouds (PCs) produced and, on the algorithms used to analyse the PCs to implement the required tasks e.g., detection, classification, and tracking.

In recent years, several studies exploiting emulation techniques to simulate and even compensate for the effects of fog through data analysis and AI have been proposed [7]-[9]. If, on the one hand, mathematical modelling and numerical simulation allow the analysis of complex scenarios and specific fog distributions, on the other, they suffer from some significant critical issues and limitations. One of the main ones is linked to the fact that the hardware and software characteristics of LiDARs are generally known only in a very approximate way. Thus, even in the hypothesis that the modelling or simulation perfectly replicated the beam propagation in bad weather, that is, what happens outside the LiDAR, there would remain significant uncertainty and arbitrariness in estimating how the LiDAR under consideration would exactly perform, given that both the characteristics of the emitted beam and the characteristics of the receiving hardware and processing software are generally little known. Such also significantly limits

the possibility of using mathematical modelling and numerical simulation for benchmarking. In this regard, the most effective strategy is reasonably experimental verification. Experimental verification of adverse weather effects on automotive LiDARs can be very challenging and, thus, potentially require highly complex structures, especially for fog.

Reasonably, the best is placing the LiDAR under test in an environment large enough to allow the designed targets to be positioned at the distances of interest. Then, such a test facility must be able to generate fog at the concentration required to give rise to the desired meteorological visibility. The complexity and costs of such facilities are such that only a few exist in the world. For example, there are plants with these characteristics in France, the CEREMA's Adverse Weather Facility in Clermont-Ferrand (www.cerema.fr), and in Japan, the Weather Chamber at the Japan Automobile Research Institute (JARI, www.jari.or.jp). Complex facilities can also be found in Germany, such as the Bosch research campus in Renningen and the CARISSMA research and testing center at the Technische Hochschule in Ingolstadt. Thanks to these facilities, some studies on the characterisation of LiDAR for automotive applications in the presence of fog have been possible e.g., [10]-[14].

In addition to the costs related to the size of these test facilities, a critical aspect is the fog. Indeed, generating a fog uniform in space over the entire volume required to allow placing the targets at distances significant for automotive applications is extremely difficult, if not impossible. In this regard, however, it is appropriate to observe that, as described in greater detail in section 2, in the hypothesis of a purely absorbing medium, the spatial uniformity of the fog along the optical path that separates the LiDAR from the target is not required as the overall attenuation suffered by each beam is given by the integral of the attenuation along its optical path. By eliminating the requirement that the fog be uniform along the entire optical path of the beams, the approximation of a purely absorbing medium makes it technically possible to use the ample facilities previously described, facilities for which it would be reasonably practically impossible to generate and guarantee the spatial uniformity of the fog.

In light of such an approximation, in this study, we propose a much simpler and cheaper setup based on the generation of fog inside a chamber with transparent walls, the fog chamber, FC. The proposed method thus implies interposing such a FC between the LiDAR under test and the target of interest. Then, to fill the FC with fog to realize the desired meteorological visibility.

As described in more detail in the following sections, such a FC was designed with dimensions small enough to obtain a setup with low costs and simple to build and use. Conversely, the FC is sufficiently large to allow attenuation of a large portion of the field-of-view, FOV, of the LiDAR under test and, therefore, to allow the analysis of extended targets as required by automotive applications.

In the following, section 2 recalls the main theoretical aspects underlying the proposed method. Then, section 3 describes the setup, measurement method, and metrics proposed for the analysis and comparison of LiDARs and PC processing algorithms. To provide an idea of the results obtainable using the proposed method, section 4 reports some example results from a popular commercial LiDAR, the VLP 16 by Velodyne, and the `pcfitsphere` function of the MATLAB® Computer Vision Toolbox. In this paper, we propose an analysis example for a single LiDAR-algorithm pair, as we wanted to focus more on the measurement approach than the results. As will be discussed in section 4, these LiDAR and algorithm are chosen because they are widely used in automotive applications.

Finally, section 5 discusses the proposed method by comparing it with the state of the art and, section 6 reports some conclusions.

2. THEORY

To allow fog to be treated both from the point of view of modelling and experimental verification, a commonly introduced approximation is to model it as if it is a purely absorbing medium. This approximation is, for example, the basis of the concept of meteorological optical visibility, MOR, defined by the World Meteorological Organization (WMO). As described above, such an approximation also makes technically feasible the use of the extensive facilities described previously for the characterisation of automotive LiDAR in the presence of fog. According to the Lambert–Beer law, the irradiance of a monochromatic and collimated beam propagating in a purely absorbing medium is given by [15], [16]:

$$E(z^*) = E(0) \cdot \exp\left[-\int_0^{z^*} \varepsilon(\lambda) \cdot c(z) dz\right], \tag{1}$$

where z is the axis along which the beam propagates, $E(z^*)$ is the irradiance at z^*, $E(0)$ is the irradiance at $z = 0$, $\varepsilon(\lambda)$ is the molar extinction coefficient at wavelength λ and, $c(z)$ is the concentration of the absorbing species, i.e., the chromophore, at z. From (1), it is easy to observe that the attenuation introduced by a purely absorbing medium depends on the average concentration of the absorbing species along the optical path

$$c_{0\mapsto z^*} = \frac{1}{z^*}\int_0^{z^*} c(z)\,\mathrm{d}z \tag{2}$$

but not on how such a chromophore distributes along the path. Therefore, for a purely absorbing medium, a uniform distribution of fog of concentration $c_0 \mapsto z^*$, as well as any other distribution of fog such as to give rise to the same average concentration $c_0 \mapsto z^*$, produce exactly the same beam attenuation. Hence, the Lambert Beer law is often reported in the form:

$$E(z^*) = E(0) \cdot \mathrm{e}^{\varepsilon \cdot c_{0\mapsto z^*} \cdot z^*}. \tag{3}$$

In light of this, in many fields ranging from avionics to automotive, the atmospheric visibility is quantified exploiting the meteorological optical range (MOR) [17]. Recalling the definition proposed by the World Meteorological Organization (WMO) [17], the ISO 289021:2012 standard [18] defines the MOR as: "*length of path in the atmosphere required to reduce the luminous flux in a collimated beam from an incandescent lamp, at a colour temperature of 2700 K, to 5 % of its original value*". From (3), the MOR can be calculated imposing [17], [18]:

$$0.05 = \mathrm{e}^{-\varepsilon \cdot c_{0\mapsto z^*} \cdot MOR}, \tag{4}$$

thus, the MOR can be expressed as:

$$MOR = \frac{1}{\sigma}\ln\frac{1}{0.05} \approx \frac{3}{\sigma}, \tag{5}$$

where σ is generally referred to as the absorption coefficient or, extinction coefficient.

As will be described later, in this study, we wanted to analyse the attenuation suffered by the beam emitted by the specific LiDAR under test. Therefore, the MOR is calculated at the wavelength used by the LiDAR under test. From (5), in this study, the MOR thus represents the path length in a uniform medium having an extinction coefficient equal to σ, required to reduce the intensity of a monochromatic collimated beam having the same wavelength as the IUT to 5 % of its original value.

3. MATERIALS AND METHODS

As introduced above, the proposed method takes advantage of the fact that, for a purely absorbing medium, the beam attenuation does not depend on the specific spatial distribution of the chromophores, but only on $c_0 \mapsto z^*$, the average concentration along the optical path. Thanks to this, we propose a method that consists in concentrating the fog only in a section of the optical path of the beam, the fog chamber. For a purely absorbing medium, the alteration of the beam caused by the propagation through the FC is exactly the same as would be obtained if the beam had propagated through a uniform fog of concentration $c_0 \mapsto z^*$. In the following, subsections 3.1 and 3.2 describe the proposed setup and measurement procedure, respectively. Finally, subsection 3.3 describes the metrics proposed for the analysis and comparison of both LiDARs and PC processing algorithms.

3.1. The proposed setup

As introduced previously, the proposed method is based on the generation of fog within a FC, which must be placed between the LiDAR under test (instrument under test, IUT) and the target of interest to generate the MOR to be analysed. As demonstrated in our previous articles [19], [20], in this way, the target can be placed at a considerable distance, without the need to generate fog along the entire optical path that separates the IUT from the target. Given the dual interest both in the characterisation and comparison of the performances of LiDARs and algorithms used to analyse the PCs provided by the LiDAR, the proposed setup must allow the analysis of the effect that the fog has on the entire target of interest. Consequently, as introduced previously, the FC must have dimensions, on the one hand, small enough to obtain a setup with low costs and simple to build and use. On the other hand, sufficiently large to allow attenuation of a large portion of the field-of-view, FOV, of the IUT to involve all the beams that contribute to the formation of the target image in the PC. The example results that will be shown in section 4 were obtained using a cubic FC with a side of 1 m.

Figure 1 shows a schematic representation of the proposed setup. As shown in the figure, the FC is placed at a distance d_{FC} from the IUT and slightly tilted by an angle α to prevent the faint specular reflection generated by the transparent walls of the FC from being detected by the IUT. The target is then positioned at a distance d_T from the IUT.

To allow the estimation of the attenuation introduced by the FC and, therefore, of the equivalent MOR, the FC is equipped with a LASER diode, LD, and a photodiode, PD. Since $\varepsilon(\lambda)$, the molar extinction coefficient at wavelength λ, depends on the wavelength, LD must be chosen with a wavelength as close as possible to that of the IUT. The beam generated by the LD is then collimated and aligned to impact the active area of PD.

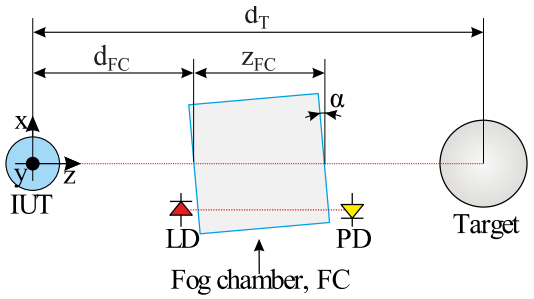

Figure 1. Schematic and not to scale representation of the proposed setup. The fog is generated inside the FG, which is placed between the IUT and the Target. To allow the MOR to be estimated, the FC is equipped with a LASER diode, LD, and a photodiode, PD. To prevent the faint specular reflection generated by the transparent walls of the FC from reaching the IUT, the FC is slightly inclined at an angle α. Therefore, the optical path length within the FC, z_{FC}, is equal to the size of the FC, rescaled by the sine of the tilt angle, α. The target and FC are located at distances d_T and d_{FC} from the IUT, respectively.

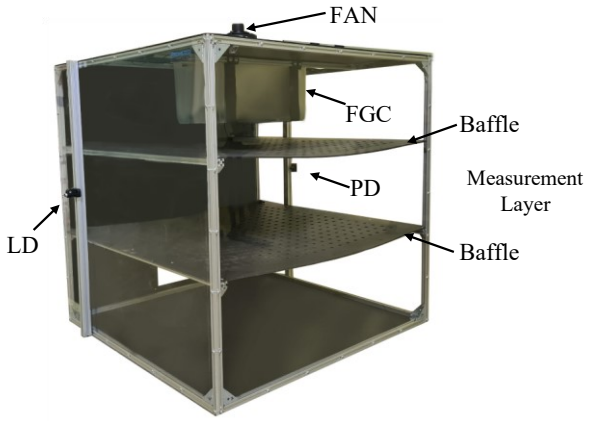

Figure 2. Picture of the developed FC. The fog is generated inside the fog generation chamber, FGC, and its distribution is promoted by two perforated baffles. The LASER diode, LD, and a photodiode, PD, circled in red, allow estimating the attenuation introduced by the FC, thus the equivalent MOR.

As shown in Figure 2, the fog is generated using an ultrasonic mist maker placed inside the fog generation chamber, FGC, placed on the top of FC.

The fog generated by the FGC is then spread into the FC using a fan. As shown in Figure 2, the FC also includes two perforated baffles to support fog uniformity. These perforated baffles create three layers: the top layer, the measurement layer, and the bottom layer. The fog generated by the FGC accumulates in the top layer from where it diffuses in the measurement layer (the middle layer). Finally, the fog in the measurement layer diffuses into the bottom layer, where a small opening allows venting of the chamber.

3.2. The proposed measurement procedure

The proposed measurement procedure consists of four phases:

1) warm-up,
2) baseline,
3) filling of the FC, and
4) measurement.

During the warm-up phase, the FGC is turned off, i.e., there is no fog generation, and the IUT is turned on for a time not less than the warm-up time determined as described in [4]. The warm-up phase also allows the LD source and the electronics for the conditioning and acquisition of the signal generated by PD to stabilize.

At the end of the warm-up phase, the baseline phase begins. During this phase, the FGC is kept off, while N_{base} PCs and recordings of the current photogenerated by the PD are acquired. Once the baseline phase is completed, the FC filling phase begins. During this phase, the FGC is turned on, and no measurements are acquired with the IUT, while the current, I, generated by the PD is used only to estimate the MOR.

Once the desired MOR is reached, the FGC turns off, and the fourth phase, the measurement phase, begins.

The measurement phase involves acquiring N_{rep} PCs in rapid succession (acquisition frequency f_{rep}). During these acquisitions, the current I generated by PD is also recorded. Once the acquisition of the N_{rep} PCs has been completed, the procedure requires waiting for a time t_{idle}. After t_{idle}, other N_{rep} PCs are acquired, simultaneously recording the current I. This routine of acquiring the N_{rep} samples in rapid succession, then waiting for t_{idle}, is repeated until the desired number of samples has been acquired. If interested in a large number of samples, the FC can be filled with fog again to repeat the procedure several times. The total number of samplings is indicated with N_{tot}; therefore, the total number of PCs available for analysis is $N_{\mathrm{tot}} \cdot N_{\mathrm{rep}}$.

In accordance with what is reported in section 2, the MOR relating to the i^{th} acquisition is equal to:

$$MOR(i) = \frac{1}{\sigma(i)} \ln\left(\frac{1}{0.05}\right), \tag{6}$$

where, $\sigma(i)$, the absorption coefficient relating to the i^{th} acquisition:

$$\sigma(i) = \frac{1}{z_{\mathrm{FC}}} \ln\left[\frac{E(0,i)}{E(z_{\mathrm{FC}},i)}\right], \tag{7}$$

being $E(0,i)$ and $E(z_{\mathrm{FC}},i)$ the irradiances entering and leaving the FC during the i^{th} acquisition. Assuming that the source is stable (experimentally verified condition) and given that, in the absence of fog inside the FC, the irradiance is conserved, $E(0,i)$ can be estimated from the irradiance leaving the FC during the baseline acquisitions. Therefore, since the current photogenerated by the PD photodiode is proportional to the irradiance leaving the FC, $E(z_{\mathrm{FC}})$, if the active area of the photodiode is larger than the spot size, the absorption coefficient relating to the i^{th} acquisition can be calculated as:

$$\sigma(i) = \frac{1}{z_{\mathrm{FC}}} \ln\left[\frac{I_{\mathrm{base}}}{I(i)}\right], \tag{8}$$

where, I_{base} and, $I(i)$ are respectively the currents recorded during the baseline phase and the i^{th} acquisition. Thus,

$$MOR(i) = z_{\mathrm{FC}} \cdot \left\{\ln\left[\frac{I_{\mathrm{base}}}{I(i)}\right]\right\}^{-1} \cdot \ln\left(\frac{1}{0.05}\right). \tag{9}$$

To minimize the contribution of ambient lighting on the photogenerated current, the photodiode is shielded from ambient lighting. Any offset is estimated and compensated by recording the current photogenerated by the PD photodiode when the LD source is obscured.

3.3. Metrics proposed for the analysis and comparison of LiDARs and processing algorithms

As previously anticipated, the proposed method allows both analysing and comparing the LiDARs performance estimating and comparing the performance of the PC processing algorithms. In this regard, the proposed method involves comparing the results obtained in the absence of fog with those obtained in fog. The metrics proposed for the analysis and comparison of LiDARs focus on the analysis of the "raw" PC, while those aimed at the analysis and comparison of the algorithms focus on the results of the processing. In both cases, the proposed method does not impose constraints on the target. If a target of specific interest is not defined, a sphere is a good choice as target since it presents significant practical advantages both in terms of alignment and processing. The results reported in section 4. were obtained by analysing a spherical target.

3.3.1. Analysis and comparison of LiDARs

For the analysis and comparison of the performance of LiDARs, it is possible to exploit the fact that LiDARs analyse the surrounding space by sampling it in spherical coordinates, generally along pre-established and constant directions, i.e., fixed elevation and azimuth angles, hereinafter referred to as rays [4].

Since the elevation and azimuth angles along which the LiDAR samples the surrounding space are fixed, for each of the rays that sample the target, the only quantity that can vary is the spherical coordinate radius, r [4]. Therefore, by analysing the PC in spherical coordinates, not only is it easy to segment the PC to consider only the rays relating to the target, but it is also possible to evaluate how the presence of fog has impacted each of the rays that made up the image of the target in the PC. Hence, for the analysis and comparison of the performance of LiDARs, it is possible to analyse parameters such as the variation of the coordinates of the centroid defined by the points of the PC relative to the target, as well as, to analyse, for each of the rays that constitute the target, the variation of the estimated axial distance, i.e., the spherical coordinate radius, r . The centroid of a finite set of k points $[p_1, p_2, \ldots, p_k]$ is the sum of all point coordinates divided by the number of points:

$$C_{\mathrm{PC}} = \frac{p_1 + p_2 + \cdots + p_k}{k}. \tag{10}$$

Assuming that the image of the target in the PC is the result of sampling carried out along k rays, thus composed of k points, from each PC it is possible to extract the centroid of the target. Therefore, to compare the behaviour of the LiDAR in the absence and presence of fog, it is possible to calculate and analyse:

- $\overline{C_{\mathrm{RAW-base}}}$ defined as the centroid of the N_{base} centroids each obtained from the N_{base} PCs relating to the baseline phase,
- $s_{\mathrm{C-RAW-base}}$ defined as the experimental standard deviation of the mean calculated from the N_{base} centroids relating to the baseline phase,
- $\overline{C_{\mathrm{RAW-meas}}(i)}$ defined as the centroid of the N_{rep} centroids each obtained from the N_{rep} PCs relating to the i^{th} acquisition recorded during the measurement phase,
- $s_{\mathrm{C-RAW}}(i)$ defined as the experimental standard deviation of the mean calculated from the N_{rep} centroids relating to the i^{th} acquisition recorded during the measurement phase.

Hence, it is possible to calculate the module of the displacement vector between the coordinates of the centroid relating to the baseline, and that relating to the i^{th} acquisition:

$$\Delta_{\mathrm{C-RAW}}(i) = |\overline{C_{\mathrm{RAW}}}(i) - \overline{C_{\mathrm{RAW-base}}}|, \quad (11)$$

and check the significance by comparing it with $s_{\mathrm{C-RAW-base}}$ and $s_{\mathrm{C-RAW}}(i)$.

Similarly, assuming that Γ is the subset of k rays, i.e., pairs of angles (φ_l, θ_m) of $l = \{1, 2, \dots, L\}$ elevation and $m = \{1, 2, \dots, M\}$ azimuthal position, that constitute the points of the PC relating to the target, for each of such k pairs is possible to evaluate the variation of the spherical coordinate, r, as the fog concentration varies. Hence, for each of the k rays that compose the image of the target in the PC, it is possible to define:

- $\overline{r_{\mathrm{RAW-base}}}(\varphi_l, \theta_m)$ as the mean value of the radius of the (φ_l, θ_m) ray calculated over the N_{base} PCs relating to the baseline phase,
- $s_{\mathrm{r-RAW-base}}(\varphi_l, \theta_m)$ as the experimental standard deviation of the mean of the radius of the (φ_l, θ_m) ray calculated over the N_{base} PCs relating to the baseline phase,
- $\overline{r_{\mathrm{RAW}}}(\varphi_l, \theta_m, i)$ as the mean value of the radius of the (φ_l, θ_m) ray calculated over the N_{rep} PCs relating to the i^t acquisition recorded during the measurement phase,
- $s_{\mathrm{r-RAW}}(\varphi_l, \theta_m, i)$ as the experimental standard deviation of the mean of the radius of the (φ_l, θ_m) ray calculated over the N_{rep} PCs relating to the i^{th} acquisition recorded during the measurement phase.

Then, for each of the $i \in [1, N_{\mathrm{tot}}]$ acquisitions, it is possible to calculate the root-mean-square error:

$$RMSE_{\mathrm{RAW}(i)} = \sqrt{\frac{\zeta(i)}{k}}, \quad (12)$$

where

$$\zeta(i) = \sum_{(\varphi_l, \theta_m) \in \Gamma} [\overline{r_{\mathrm{RAW}}}(\varphi_l, \theta_m, i) - \overline{r_{\mathrm{RAW-base}}}(\varphi_l, \theta_m)]^2, \quad (13)$$

and k is the number of rays sampling the target and, therefore, the cardinality of the subset Γ — the subset of rays, i.e., pairs of angles (φ_l, θ_m) that constitute the points of the PC relating to the target.

3.3.2. Analysis and comparison of PC processing algorithms

For the analysis and comparison of PC processing algorithms, it is possible to proceed similarly to what was done for the analysis and comparison of LiDARs. The difference is that the analysis and comparison of LiDAR is based on PCs, i.e., raw data, while the analysis and comparison of processing algorithms must take into consideration the outputs of the processing algorithms.

Given that PC processing algorithms are generally aimed at tasks such as detection, classification, and tracking, a quantity of interest is the ability to continue performing these tasks even in the presence of fog. It is thus convenient to define the Boolean parameter "SUCCEEDED(MOR)" whose value is:

- 1 if the algorithm was able to carry out the task while maintaining an error lower than or equal to the maximum error allowed, or,
- 0, if the algorithm was not capable of carrying out the task or has carried out it by introducing an error greater than the maximum allowed error.

Moreover, similarly to before, it is possible to calculate and analyse:

- $\overline{C_{\mathrm{ALG-base}}}$ as the centroid of the N_{base} centroids each obtained by applying the processing algorithm to the N_{base} PCs relating to the baseline phase,
- $s_{\mathrm{C-ALG-base}}$ as the experimental standard deviation of the mean calculated from the N_{base} centroids relating to the baseline phase,
- $\overline{C_{\mathrm{ALG-meas}}}(i)$ as the centroid of the N_{rep} centroids each obtained by applying the processing algorithm to the N_{rep} PCs relating to the measurement phase,
- $s_{\mathrm{C-ALG}}(i)$ as the experimental standard deviation of the mean calculated from the N_{rep} centroids relating to the i^{th} acquisition recorded during the measurement phase.

Hence, it is possible to calculate the module of the displacement vector between the coordinates of the centroid relating to the baseline, and that relating to the i^{th} acquisition:

$$\Delta_{\mathrm{C-ALG}}(i) = |\overline{C_{\mathrm{ALG}}}(i) - \overline{C_{\mathrm{ALG-base}}}|, \quad (14)$$

and check the significance by comparing it with $s_{\mathrm{C-ALG-base}}$ and $s_{\mathrm{C-ALG}}(i)$.

Similarly to what was done previously, if the output of the processing algorithm includes a surface, it is possible to compare the surface relating to the baseline with that relating to the i^{th} acquisition and calculate the root-mean-square error, $RMSE_{\mathrm{ALG}}(i)$. If the target is a sphere, the PC processing algorithm must reasonably be aimed at identifying a sphere, thus extracting its parameters, center, and radius of the sphere. $\Delta_{\mathrm{C-ALG}}(i)$ then becomes the magnitude of the difference between the average coordinates of the centre of the sphere during the i^{th} acquisition and during the baseline. The calculation of $RMSE_{\mathrm{ALG}}(i)$ is further simplified as it is equal to the difference between the average radius of the sphere extracted from the i^{th} acquisition and the average radius of the sphere obtained during the baseline.

4. RESULTS

As previously introduced, to provide an idea of the results obtainable using the proposed method, this section reports some example results obtained from a very popular LiDAR in the automotive sector, namely, the VLP16 from Velodyne whose PCs were analysed using a popular and easily available processing algorithm, that is, the `pcfitsphere` function of the MATLAB® Computer Vision Toolbox. Such an algorithm is based on the Mestimator Sample Consensus (MSAC) algorithm to find the sphere, which is a variant of the RANdom SAmple Consensus (RANSAC) algorithm. This algorithm was chosen because it is a popular choice for object detection [21]-[23] and because it is available in the MATLAB® toolboxes and, therefore, usable by anyone wishing to repeat the test.

The target used in these tests was a polystyrene sphere with a radius of 15 cm. During the tests, the sphere was kept suspended by a thin wire. Table 1 summarizes the settings used to acquire the reported example results. As an example, Figure 3 shows a PC acquired during the baseline phase (no fog along the optical path), while Figure 4 shows a zoom of the sampling of the target in such a PC. Depending on the applications of interest, the detection success can be accomplished in case the error is lower than a specific threshold T.

Table 1. Settings used to acquire the reported example results.

Setting	Value
N_{base}	10
N_{rep}	5
f_{rep}	10 Hz
t_{idle}	60 s
N_{tot}	1500
d_{T}	≈ 2.75 m
d_{FC}	≈1 m
Target sphere radius	15 cm
Target sphere material	polystyrene

Defining:

$$\Delta_{\text{C-ALG-\%}}(i) = |\overline{C_{\text{ALG}}}(i) - \overline{C_{\text{ALG-base}}}| \cdot 100, \quad (15)$$

and

$$RMSE_{\text{ALG-\%}}(i) = \frac{|\overline{R_{\text{sph}}}(i) - \overline{R_{\text{sph-base}}}|}{R_{\text{sph-base}}} \cdot 100, \quad (16)$$

where $R_{\text{sph}}(i)$ and $R_{\text{sph-base}}$ are the average radius of the sphere extracted from the i^{th} acquisition and the average radius of the sphere obtained during the baseline, respectively, the target detection was considered successful, i.e., "SUCCEEDED=1", if

$$\Delta_{\text{C-ALG-\%}}(i) \leq T_{\Delta C}\,, \quad (17)$$

and

$$RMSE_{\text{ALG-\%}}(i) \leq T_{\text{RMSE}}. \quad (18)$$

Figure 5 shows the trend of the Boolean parameter "SUCCEEDED" obtained from the analysis of the outputs of the `pcfitsphere` function as the MOR generated by the FC varies. Figure 6 and Figure 7 show the trends of $\Delta_{\text{C-ALG-\%}}(i)$ and $RMSE_{\text{ALG-\%}}(i)$, also reporting the respective experimental standard deviation of the mean.

For example, considering a maximum acceptable error $T = 20$ %, Figure 5 shows the trend of SUCCEEDED parameter for the sphere Radius and Center coordinates. As particularly evident from Figure 6, the failure in the detection of the sphere, i.e., SUCCEEDED = 0, is mainly due to the error in estimating the coordinates of the center of the sphere. Indeed, when the MOR drops below approximately 3 m, the processing algorithm appears to be no longer able to reconstruct the sphere. The analysis of the PCs, i.e., the RAW data provided by the IUT, reveals that this is because, for a MOR lower than about 3 m, the LiDAR begins detecting the fog front as a target. Indeed, when the MOR drops below approximately 3 m, the centroid of the target was substantially in correspondence with the fog front, i.e. at distance d_{FC} from the IUT.

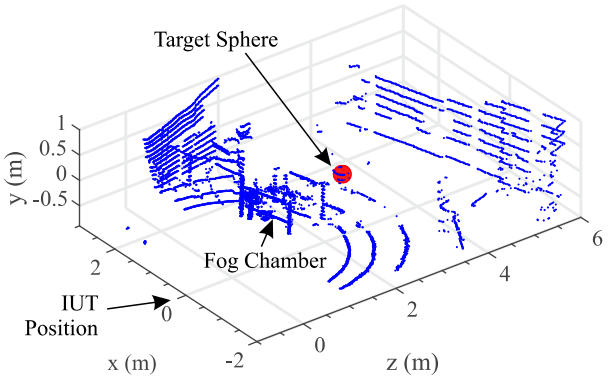

Figure 3. PC acquired during the baseline phase (no fog along the optical path). A red sphere has been inserted into the image whose radius and centre correspond to the average radius and average centre recorded during the baseline phase. In the figure, it is also possible to see the metal frames of the FC (the rectangles located approximately 1 m and 2 m from the IUT). The IUT position corresponds to coordinates (0,0,0).

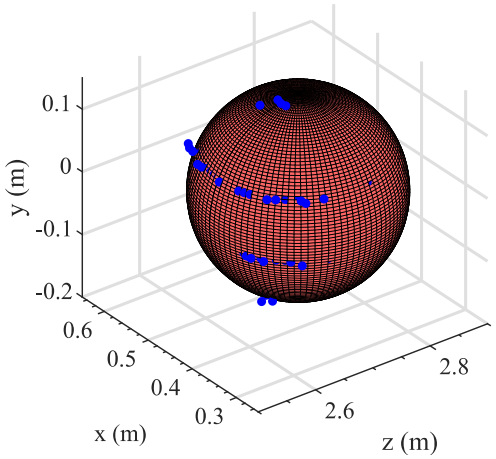

Figure 4. Zoom of the sampling of the target relating to the PC shown in Figure 3. In the figure, it is possible to observe how the points of the PC, represented with blue dots, accurately intercept the surface of the sphere.

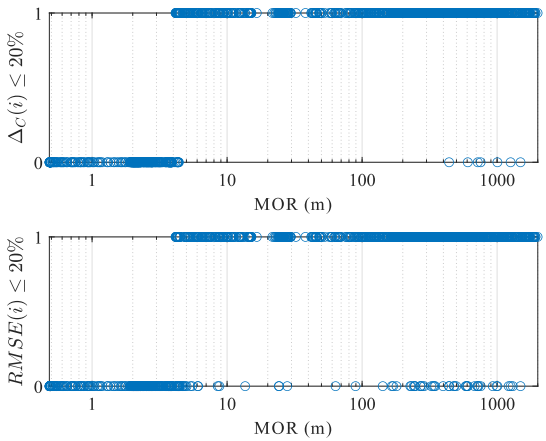

Figure 5. Trend of the Boolean parameter "SUCCEEDED" obtained from the analysis of the outputs of the `pcfitsphere` function as the MOR generated by the FC varies.

5. DISCUSSION

As described previously, mathematical models or numerical simulations can be used to analyse the performance of LiDARs in the presence of fog. Although such approaches allow for overcoming some relevant issues related to experimentation, they are not free of significant drawbacks and limitations.

As introduced previously, the LiDAR response also depends on the shape and amplitude of the echo received. These characteristics depend on countless quantities both internal to the LiDAR and external. For example, the shape and amplitude of the received pulse depend on external quantities such as the inclination and reflectance of the specific point of the target on which the beam generated by the LiDAR is incident [24]. The

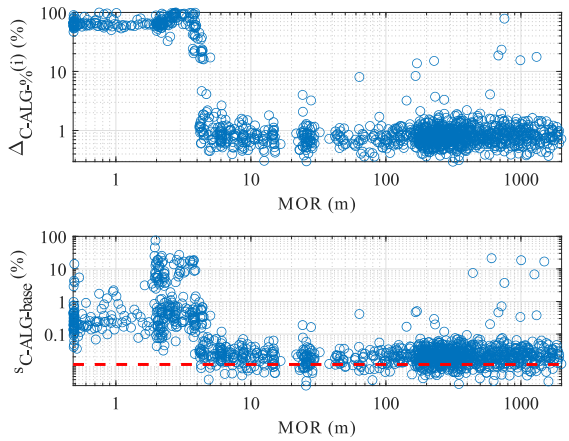

Figure 6. $\Delta_{C-ALG-\%}(i)$ and $s_{C-ALG}(i)$ as a function of MOR. In the lower figure, the dashed red line (– – –) represents $s_{C-ALG-base}$.

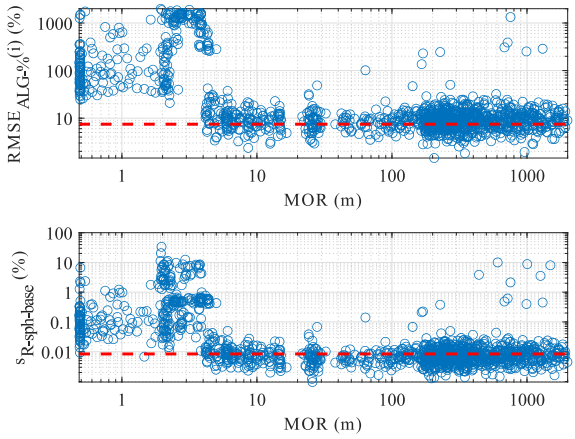

Figure 7. $RMSE_{ALG-\%}(i)$ and $s_{R-sph}(i)$ as a function of MOR. In the upper figure, the dashed red line (– – –) represents the RMSE on the baseline radius obtained by replacing in the (16) $R_{sph}(i)$ with $R_{sph-base}$ and $R_{sph-base}$ with the actual radius of the sphere $R = 15$ cm. In the lower figure, the dashed red line (– – –) represents $s_{R-sph-base}$.

greatest criticality, however, is because, in addition to the significant complexity linked to the modelling of the propagation and reflection of the beams, much of the information required to estimate or simulate the signal photogenerated from the LiDAR detectors is often partial or even completely unknown. Indeed, in addition to the characteristics of the transmission medium, the shape (time evolution) of the pulse generated by the LiDAR detector in response to the received echo depends on a multitude of characteristics of the LiDAR itself such as the space-time characteristics of the emitted impulse, the field of view (FOV), the aperture stop and, the responsivity of the detectors, as well as, the performance of the front-end electronics. When these characteristics are known, they are generally only approximately known.

Even in the fortunate hypothesis of being able to analytically describe or numerically model in an appropriate way the temporal evolution of the received echo, the analysis that the LiDAR operates on this signal to compose the PC is reasonably fully known only to the manufacturer.

Hence, mathematical modelling and numerical simulation are inexorably significantly limited by the incomplete knowledge of the LiDAR to be analysed. The hypotheses and assumptions necessary to overcome this lack of information thus make, on the one hand, the estimate of the actual performance less accurate, and on the other hand, the benchmarking of the performance of different LiDARs complex, if not impossible. By using the LiDAR intended to be analysed, experimentation does not require knowing any of the previous information. Experimental verification thus appears reasonably more capable of allowing benchmarking. However, also experimentation presents significant complexities. The main one is the generation of fog. Nonetheless, in the hypothesis of a purely absorbent medium, the spatial distribution of the fog becomes irrelevant since the attenuation suffered by the beam depends only on the average concentration of the fog along its optical path and not on how fog distributes along it. Such an approximation is the basis of the proposed method, as well as of the ample facilities described previously for the characterisation of automotive LiDAR in the presence of fog.

In conclusion, mathematical models or numerical simulations allow the effect of different fog patterns to be analysed quite accurately. The main limitation of these approaches is that, since the characteristics of LiDARs are generally known only approximately, it is difficult to accurately analyse performance, as well as compare different LiDARs as, in general, the information required to highlight any differences is not fully available.

On the contrary, experimental verification encounters significant complications in the analysis of complex fog patterns but, does not require knowledge of any information to compare the behaviour of the LiDARs since what is analysed is the actual signal obtained.

6. CONCLUSIONS

Driven by the goal of autonomous driving, recent years have seen a proliferation of LiDAR systems for automotive applications. This has led to an increasing need for measurement methods capable of evaluating and comparing as well as guiding the development of both the LiDARs and, the algorithms responsible for analysing the PCs provided by the LiDARs.

Driven by this request, many methods and studies have been proposed. However, most of these methods and studies have focused on the analysis and comparison of the performances obtained in conditions of good visibility. In this study, we propose a simple and cost-effective method for the analysis and comparison in the presence of fog. Such a method allows both to analyse and compare the LiDARs performance and to analyse and compare the performance of the PC processing algorithms.

The proposed method is based on generating the fog inside an FC, that is, inside a chamber with transparent walls. Such a method allows analysing and comparing, as well as supporting the development of both the LiDARs and the PC processing algorithms. The example results reported in section 4 demonstrate how the proposed method can analyse both the performance of the algorithms and of the LiDARs. For example, the proposed method allowed determining the maximum fog concentration, i.e., the minimum MOR, beyond which the algorithm was no longer able to operate correctly. Moreover, the proposed method also allowed us to discover the cause of the algorithm error, that is, the fact that, as the fog concentration increases, the IUT incorrectly starts to recognize the fog front as a target.

As introduced in section 1, although it involves critical issues in terms of complexity and costs, the best is reasonably to place the LiDAR and the target in an environment filled with fog, i.e.

inside the FC. The proposed setup has limitations primarily due to the approximations intrinsic in its approach based on the purely absorbing medium. There are some several limitations due to the hardware used in this prototype. For example, at present, visibility is estimated using a single pair of LD and PD, thus sampling the FC volume along a single line. Moreover, as introduced in section 1, the best is to place the LiDAR directly inside the FC, to perform a test the most similar to the reality. However, future studies could focus on configuration improvements to overcome hardware limitations. For example, a matrix of LD-PD pairs could be implemented to monitor visibility at different points of the FC volume.

Despite the previous limitations, the proposed method allows analysing and comparing the performance of both LiDARs and PC processing algorithms in the presence of fog, all while avoiding both the cost and complexity of the ample facilities and the limitations intrinsic to mathematical modelling and numerical simulation.

REFERENCES

[1] F. Wang, Y. Zhuang, H. Gu, H. Hu, Automatic generation of synthetic lidar point clouds for 3-d data analysis, IEEE Transactions on Instrumentation and Measurement, vol. 68, 2019, no. 7, pp. 2671– 2673.
DOI: 10.1109/TIM.2019.2906416

[2] J. Lambert, A. Carballo, A. M. Cano, P. Narksri, D. Wong, E. Takeuchi, K. Takeda, Performance analysis of 10 models of 3d lidars for automated driving, IEEE Access, vol. 8, 2020, pp. 131 699–131 722.
DOI: 10.1109/ACCESS.2020.3009680

[3] S. Cattini, D. Cassanelli, L. D. Cecilia, L. Ferrari, L. Rovati, A procedure for the characterization and comparison of 3-D LiDAR systems, IEEE Transactions on Instrumentation and Measurement, vol. 70, 2021, pp. 1–10.
DOI: 10.1109/TIM.2020.3043114

[4] S. Cattini, D. Cassanelli, G. D. Loro, L. D. Cecilia, L. Ferrari, L. Rovati, Analysis, quantification, and discussion of the approximations introduced by pulsed 3-D LiDARs, IEEE Transactions on Instrumentation and Measurement, vol. 70, 2021, pp. 1–11.
DOI: 10.1109/TIM.2021.3124038

[5] M. Rodríguez-Cortina, P. Adamiec, J. Barbero, X. Quintana, M. A. Geday, Emulation technique of multiple overlapped return echoes of a spatial lidar with 100-db dynamic resolution, IEEE Transactions on Instrumentation and Measurement, vol. 70, 2021, pp. 1–7.
DOI: 10.1109/TIM.2021.3092778

[6] S. Cattini, D. Cassanelli, L. Ferrari, L. Rovati, A method for estimating object detection probability, lateral resolution, and errors in 3-D LiDARs, IEEE Transactions on Instrumentation and Measurement, vol. 72, 2023, pp. 1–14.
DOI: 10.1109/TIM.2023.3298392

[7] M. Dreissig, D. Scheuble, F. Piewak, J. Boedecker, Survey on lidar perception in adverse weather conditions, 2023 IEEE Intelligent Vehicles Symposium (IV), 2023, pp. 1–8.
DOI: 10.1109/IV55152.2023.10186539

[8] A. Piroli, V. Dallabetta, J. Kopp, M. Walessa, D. Meissner, K. Dietmayer, Energy-based detection of adverse weather effects in lidar data, IEEE Robotics and Automation Letters, vol. 8, 2023, no. 7, pp. 4322–4329.
DOI: 10.1109/LRA.2023.3282382

[9] T. Yang, Y. Li, Y. Ruichek, Z. Yan, Performance modeling a nearinfrared tof lidar under fog: A data-driven approach, IEEE Transactions on Intelligent Transportation Systems, vol. 23, 2022, no. 8, pp. 11 227–11 236.
DOI: 10.1109/TITS.2021.3102138

[10] M. Kutila, P. Pyykönen, H. Holzhüter, M. Colomb, P. Duthon, Automotive lidar performance verification in fog and rain, 2018 21st Int. Conf. on Intelligent Transportation Systems (ITSC), Maui, HI, USA, 4-7 November 2018, pp. 1695–1701.
DOI: 10.1109/ITSC.2018.8569624

[11] Y. Li, P. Duthon, M. Colomb, J. Ibanez-Guzman, What happens for a tof lidar in fog? IEEE Transactions on Intelligent Transportation Systems, vol. 22, 2021, no. 11, pp. 6670–6681.
DOI: 10.1109/TITS.2020.2998077

[12] M. Wichmann, M. Kamil, A. Frederiksen, S. Kotzur, M. Scherl, Long-term investigations of weather influence on direct time-offlight lidar at 905nm, IEEE Sensors Journal, vol. 22, 2022, no. 3, pp. 2024–2036.
DOI: 10.1109/JSEN.2021.3133658

[13] M. Ballesta-Garcia, S. P. na Gutiérrez, A. Rodríguez-Aramendía, P. García-Gómez, N. Rodrigo, A. R. Bobi, S. Royo, Analysis of the performance of a polarized lidar imager in fog, Opt. Express, vol. 30, Nov 2022, no. 23, pp. 41 524–41 540.
DOI: 10.1364/OE.471872

[14] F. Sezgin, D. Vriesman, D. Steinhauser, R. Lugner, T. Brandmeier, Safe autonomous driving in adverse weather: Sensor evaluation and performance monitoring, 2023 IEEE Intelligent Vehicles Symp. (IV), Anchorage, AK, USA, 4-7 June 2023, pp. 1–6.
DOI: 10.1109/IV55152.2023.10186596

[15] H. Gross, Radiometry, John Wiley & Sons, Ltd, 2005, ch. 6, pp. 229–268.
DOI: 10.1002/9783527699223.ch6

[16] V. E. Zuev, Propagation of Visible and Infrared Radiation in the Atmosphere, John Wiley & Sons, 1974.

[17] W. M. Organization, Guide to Instruments and Methods of Observation, World Meteorological Organization, 2018, vol. 1.

[18] I. 289021:2012, Air quality - environmental meteorology part 1: Ground-based remote sensing of visual range by lidar, ISO — International Organization for Standardization, Geneva, Switzerland, Tech. Rep., 2012. Online [Accessed 6 December 2024]
https://www.iso.org/standard/45022.html

[19] D. Cassanelli, S. Cattini, G. Di Loro, L. Di Cecilia, L. Ferrari, D. Goldoni, L. Rovati, A simple method for the preliminary analysis and benchmarking of automotive LiDARs in fog, 2022 IEEE Int. Instrumentation and Measurement Technology Conf. (I2MTC), Ottawa, ON, Canada, 16-19 May 2022, pp. 1–6.
DOI: 10.1109/I2MTC48687.2022.9806549

[20] D. Cassanelli, S. Cattini, L. Ferrari, L. Rovati, A method for the estimate erroneous fog detection in automotive lidar, 2023 IEEE Int. Instrumentation and Measurement Technology Conf. (I2MTC), Kuala Lumpur, Malaysia, 22-25 May 2023, pp. 01–06.
DOI: 10.1109/I2MTC53148.2023.10176011

[21] P. Torr, A. Zisserman, Mlesac: A new robust estimator with application to estimating image geometry, Computer Vision and Image Understanding, vol. 78, 2000, no. 1, pp. 138–156.
DOI: https://doi.org/10.1006/cviu.1999.0832

[22] B. Wang, J. Lan, J. Gao, Lidar filtering in 3d object detection based on improved ransac, Remote Sensing, vol. 14, 2022, no. 9.
DOI: 10.3390/rs14092110

[23] I.-S. Weon, S.-G. Lee, J.-K. Ryu, Object recognition based interpolation with 3d lidar and vision for autonomous driving of an intelligent vehicle, IEEE Access, vol. 8, 2020, pp. 65 599–65 608.
DOI: 10.1109/ACCESS.2020.2982681

[24] D. Cassanelli, S. Cattini, G. D. Loro, L. D. Cecilia, L. Ferrari, L. Rovati, LiDARs detected signal and target distance estimation: measurement errors from target reflectance and multiple echos, 2022 IEEE Int. Workshop on Metrology for Automotive (MetroAutomotive), Modena, Italy, 4-6 July 2022, pp. 59–64.
DOI: 10.1109/MetroAutomotive54295.2022.9855105